Applied Mechanics and Materials *Online: 2010-06-30*
ISSN: 1662-7482, Vols. 24-25, pp 103-108
doi:10.4028/www.scientific.net/AMM.24-25.103

Analysis of the strain and stress fields of cardboard box during compression by 3D Digital Image Correlation

J. Viguié[1,a], P.J.J. Dumont[1,b], P. Vacher[2], L. Orgéas[3], I. Desloges[1], E. Mauret[1]

[1]CNRS / Institut Polytechnique de Grenoble (Grenoble INP), Laboratoire de Génie des Procédés Papetiers (LGP2), 461 rue de la Papeterie, BP 65, 38402 Saint-Martin-d'Hères cedex, France

[2]Université de Savoie, Laboratoire SYMME, Polytech Savoie, Domaine Universitaire, BP 80439, 74944 Annecy-le-Vieux, France

[3]CNRS / Institut Polytechnique de Grenoble (Grenoble INP), Laboratoire Sols-Solides-Structures-Risques (3S-R), BP 53, 38041 Grenoble cedex 9, France

[a]jeremie_viguie@yahoo.fr, [b]pierre.dumont@grenoble-inp.fr

Keywords: G-flute corrugated board, buckling behaviour, digital image correlation, strain and stress fields measurement

Introduction

Corrugated boards with small flutes appear as good alternatives to replace packaging folding boards or plastic materials due their small thickness, possibility of easy recycling and biodegradability. Boxes made up of these materials have to withstand significant compressive loading conditions during transport and storage. In order to evaluate their structural performance, the box compression test is the most currently performed experiment. It consists in compressing an empty container between two parallel plates at constant velocity. Usually it is observed that buckling phenomena are localized in the box panels, which bulge out during compression [1]. At the maximum recorded compression force, the deformation localises around the box corners where creases nucleate and propagate. This maximum force is defined as the quasi-static compression strength of the box. The prediction of such strength is the main topic of interest of past and current research works. For example, the box compression behaviour of boxes was studied by Mc Kee et al. [2] and Urbanik [3], who defined semi-empirical formula to predict the box compression strength, as well as by Beldie et al. [4] and Biancolini et al. [5] by finite element simulations. But comparisons of these models with experimental results remain rather scarce and limited.
2D Digital Image Correlation method was used to study the behaviour of a box panel [6] subjected to compression. However this method does not allow the measurement of the out-of-plane displacement which is significant when the panel buckles. It is now possible to measure the 3D displacement field and the surface strain field of any 3D object by the digital image stereocorrelation technique (DISC or 3D DIC) [7,8]. Hence, the objective of this paper is to revisit the work of [6], by using the 3D DIC technique to better estimate both the 3D displacement field and the in-plane strain field of box panels during the box compression. Furthermore, combined with the elastic orthotropic properties of the outer liner (determined elsewhere), such measurements allows the estimation of the stress field on the surface of the panels.

Materials, specimens and Experimental Procedure

G-flute corrugated board and box manufacturing. The material used in this study is a double-faced corrugated board the flutes of which have a so called G profile. Their typical dimensions are shown in Fig. 1(a). This sandwich structure has a nominal thickness *e* of 0.77 mm and an average basis weight of 450 g/m^2. It is composed of a 160 g/m^2 outer liner made up of chemical pulp (kraftliner), a 110 g/m^2 corrugated medium essentially made up of recycled pulp and a 140 g/m² inner liner made up of a mix of pulps (testliner). These papers are glued together using a starch-

based adhesive. Tested boxes are cubic with dimension 73 × 73 × 73 mm^3. As shown in Fig. 1(b), the box blank includes panels, flaps (panels covering the box), folding lines and a manufacturer joint. The crease depth was chosen equal to 1 mm. Once the box was erected and glued, the inner and outer flaps covered completely the top and bottom box surfaces. Notice that the flutes are vertical in the box panels: this means that the cross manufacturing direction (CD) of the corrugated board is aligned along the compression axis.

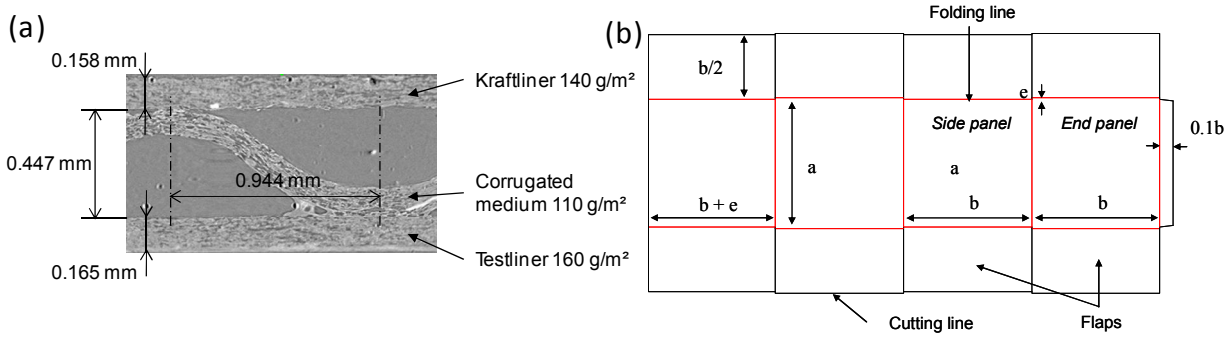

Figure 1. (a) 2D Micrograph showing the cross-section of a G-flute profile corrugated board (obtained from a 3D microtomography volume imaged at the European Synchrotron Radiation Facility (ESRF) on ID19 beamline). Note that the uniform grey zones correspond to voids. (b) Box blank.

Compression tests. Compression tests were performed with an Instron 5569 testing device at a constant compression velocity of 13 mm/min along the $\underline{\mathbf{e}}_{y'}$ direction (*cf.* Fig. 2(a)). The compression plates are made up of polished aluminium. A photograph of a box, which is placed between the compression plates before the test, is shown in Fig. 2(a). During these experiments, the compression force F and the axial plate displacement Δa were on-line recorded. This permitted to calculate the following macroscopic box axial stress Σ simply defined as

$$\Sigma = \frac{F}{S_0}, \tag{1}$$

where $S_0 = 4e(b-e)$ is defined arbitrarily as the surface of the box cross-section perpendicular to the compression axis $\underline{\mathbf{e}}_{z'}$. Similarly, a macroscopic strain ε is defined as

$$\varepsilon = \ln\left(\frac{a+\Delta a}{a}\right). \tag{2}$$

3D Digital Image Stereocorrelation technique. Two of the external panel surfaces were coated with a random pattern made of small black speckles (0.1 to 0.3 mm) obtained spraying a black paint. In order to estimate the 3D displacement field of these two surfaces, the stereocorrelation technique was used [8]. Here, this was performed with the DIC Software 7D [9]. During the compression test, two images of the deforming panels and of their superimposed speckle patterns are recorded simultaneously and sequentially by using, for stereovision, two CCD cameras (3872 × 2592 pixels), whose relative position and orientation (α angle) are known (cf. Fig. 2(c)) using a calibration procedure [10]. Then, the correspondence between two image points belonging to the pair of simultaneously recorded images was identified by applying an image correlation technique using square windows of 10 × 10 pixels and subsets of 10 × 10 pixels centred around the corners of the windows. This stage requires the minimization of a correlation function and involves interpolating the grey levels of the left and right images using bilinear interpolation functions. The error can be estimated to be lower than 0.1 pixel. Then, the 3D coordinates *x'*, *y'* and *z'*, of a physical point can be computed by triangulation. At each stage of the sequence, the principle of the surface reconstruction is similar. This allows the reconstruction of the whole surface of the studied panels, Fig. 2(d) shows this surface at the maximum compression stress (red point in Fig. 2(b)). The 3D displacement field $\underline{\mathbf{u}}(x',y',z') = u'\underline{\mathbf{e}}_{x'} + v'\underline{\mathbf{e}}_{y'} + w'\underline{\mathbf{e}}_{z'}$ of all points of the panels is measured by analysing a sequence of pair of stereo images using the image of the panels taken by the left camera

in their initial configuration (before compression) as a reference. As an example, Fig. 2(e) shows the out-of-plane displacement w' of the surface of the two studied panels in the coordinate system (x',y',z') of the left camera. Finally, in this study, the displacement field $\underline{\mathbf{u}}(x,y,z) = u\underline{\mathbf{e}}_x + v\underline{\mathbf{e}}_y + w\underline{\mathbf{e}}_z$ was expressed in the panel local coordinate system (x,y,z) (Fig. 2(f)). Thereafter, the components E_{xx}, E_{yy} and $2E_{xy}$ of the Green-Lagrange strain tensor $\underline{\underline{\mathbf{E}}}$ can be estimated. The spatial partial derivatives are calculated by using a standard centred finite difference scheme. For the calculation of the strain field, the displacement field was used in its raw form and in a smoothed form (Matlab smooth function). Fig. 2(g-h) were obtained respectively. It is worth noting that the smoothed displacement field allows a less «noisy» strain field to be obtained at the macroscopic scale. The information contained in the smooth displacement field appeared us to be satisfactory for the rest of the analysis.

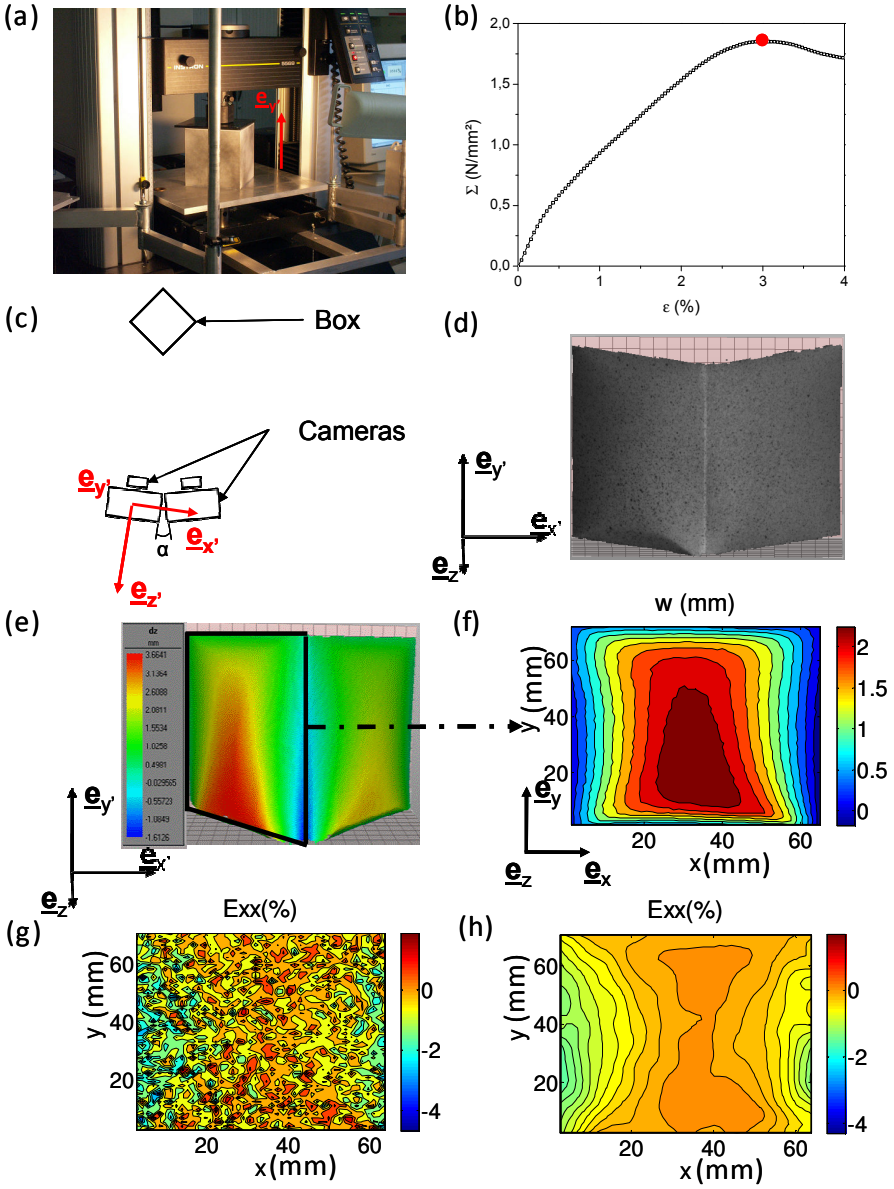

Figure 2. (a) Picture of a box in the compression setup. (b) Typical experimental curve of the box compression stress with respect to the box compression strain. (c) Scheme of the imaging setup (top view). (d) Reconstructed 3D surface (final state). (e) Component w' of the displacement field of the two studied panels in the (x', y', z') coordinate system. (f) Displacement w of the panel with outer flaps (see the arrow) in the panel coordinate system (x, y, z). (g) Component E_{xx} of the displacement field (obtained from the raw displacement field). (h) Same component when the displacement field is smoothed.

Results

Full displacement field of box panels. In this section, the stereocorrelation technique was used to describe the displacement field of a panel with outer flaps at one compression stage corresponding to macroscopic strain $\varepsilon = 3\%$. The corresponding stress-strain curve is given in Fig. 2(b). As shown in this figure, the compression strain $\varepsilon = 3\%$ corresponds to the box compression critical strain (this point is showed by a red disk in the figure). The components u, v and w of the displacement field are displayed in Fig. 3.

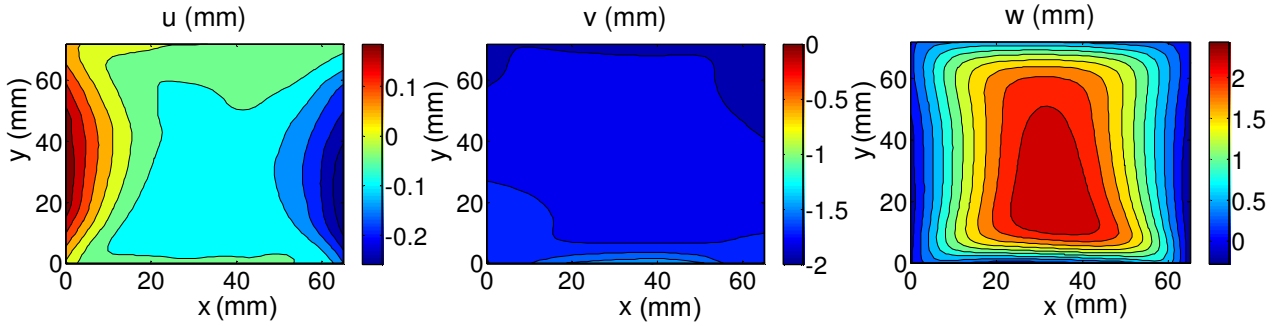

Figure 3. Maps of the components u, v and w of the displacement field of the panel with outer flaps from box with dimensions 73 × 73 × 73 mm^3 at the critical strain ($\varepsilon = 3\%$).

Firstly, it is worth noting that the displacement components are largely heterogeneous. The out-of-plane displacement w and the in-plane displacement v are of the same order and these two components are largely higher than the in-plane displacement u. This indicates clearly that the panel buckles during the compression. The maximum values of the out-of-plane component are obtained for a large zone, centred below the panel centre at the critical strain, as the values of w close to the box edges remained nearly equal to zero or were even slightly negative. Thus, high gradients for this component were found when going through the panel from its edges to the previous central zone, especially along the y-direction. The component v of this displacement field was found to be of the same order as w. But quite astonishingly, it can also be observed that this component is nearly homogeneous over the whole panel surface. This means that the panel exhibits a vertical rigid motion during the box compression. Its origin might be related to both the motion and the compression of the outer flaps joined to the panel, and more presumably to the crush of the junction scores during the compression experiment. Unfortunately, the scores are outside the correlation zones. This point could be improved in future works. The component u of the displacement field was observed to be small compared to v and w, but clearly shows that the vertical edges of the panel do not remain straight and tend to move towards the panel centre as the compression strain increases.

Strain field of box panels. By analysing closely the components of the Green-Lagrange strain tensor, it appeared that the contribution of some spatial gradients of u, v and w could be neglected. This permits to write the strain components E_{xx}, E_{yy} and $2E_{xy}$ adopting the following reduced expressions, which correspond to a von Kármán-type strain field:

$$E_{xx} \approx \frac{\partial u}{\partial x} + \frac{1}{2}\left(\frac{\partial w}{\partial x}\right)^2 ;\; E_{yy} \approx \frac{\partial v}{\partial y} + \frac{1}{2}\left(\frac{\partial w}{\partial y}\right)^2 ;\; 2E_{xy} \approx \frac{\partial u}{\partial y} + \frac{\partial v}{\partial x} + \frac{\partial w}{\partial x}\frac{\partial w}{\partial y}.$$

Figure 4 shows the components E_{xx}, E_{yy} and $2E_{xy}$ of the strain field at the critical compression strain $\varepsilon = 3\%$. Whatever these components, their values are almost equal to zero in the region of the panel centre. In contrast, along the panel edges the strain variations are more pronounced. The variations of E_{xx} are particularly important along the vertical edges of the box, whereas the variations of E_{yy} appear mainly along the horizontal edges of the panel. In both cases, these strain components have negative values, characteristic of a compressive deformation state. The maximum compressive strains are attained at the middle of the edges, and gradually decrease as the corner

region is reached. It is also interesting to notice that the compressed zones along the *x*-axis are wider than along the *y*-axis, despite this direction corresponds to the box compression axis. The compressive strain E_{yy} is indeed more localized than the E_{xx} one.

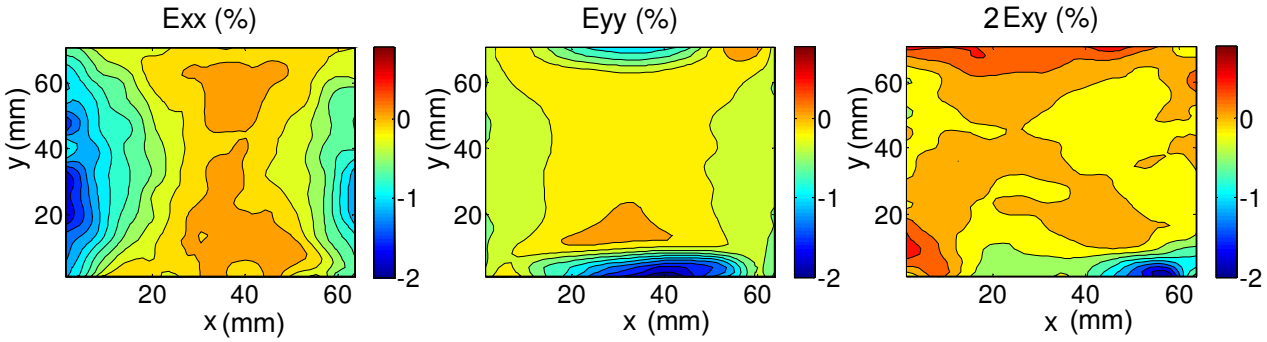

Figure 4. Components of the Green-Lagrange strain tensor at $\varepsilon = 3\%$.

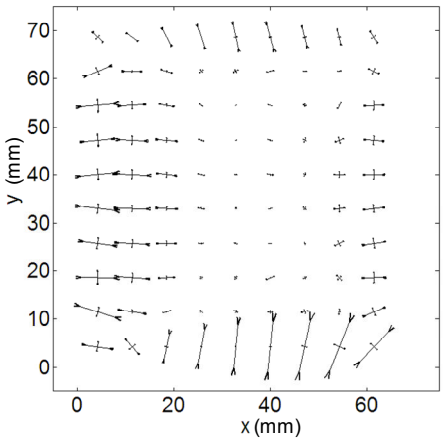

Figure 5. Map of the principal strains oriented in the principal directions of the strain tensor.

Figure 5 shows the magnitude of the principal strains and the orientation of the principal directions. It can be noticed that the principal directions almost correspond to the loading coordinate system in the zones located along the edges, whereas it is not the case in the corner regions. The regions along the vertical edges are compressed in the two directions, but the most significant values are recorded perpendicularly to the compression direction. Along the horizontal edges, only one principal strain is not equal to zero and is higher than those recorded along the vertical edges. This corresponds to a complex strain situation, which might be related to a common influence of the phenomena of compression of the flaps and crush of the horizontal scores, as well as of the neighbouring panels.

Stress field of box panels. The elastic orthotropic properties of the outer liner were determined in a previous work [11]. Combined with the strain field measurements, they allow the estimation of the in-plane stress along the compressed panels, as shown in Figure 6. The evolution of the computed stress field is very similar to that obtained for the strain field. Due to the simplicity of the used elastic model, the stress values are clearly overestimated in the regions close to the edges. But they show that the yield limit is largely exceeded in theses regions. This corresponds to an irreversible damage process of the microstructure of paper. Currently, a Tsai-Wu criterion for the elastic is being built in order to determine where the elastic limit is reached and exceeded in the panel during the box compression.

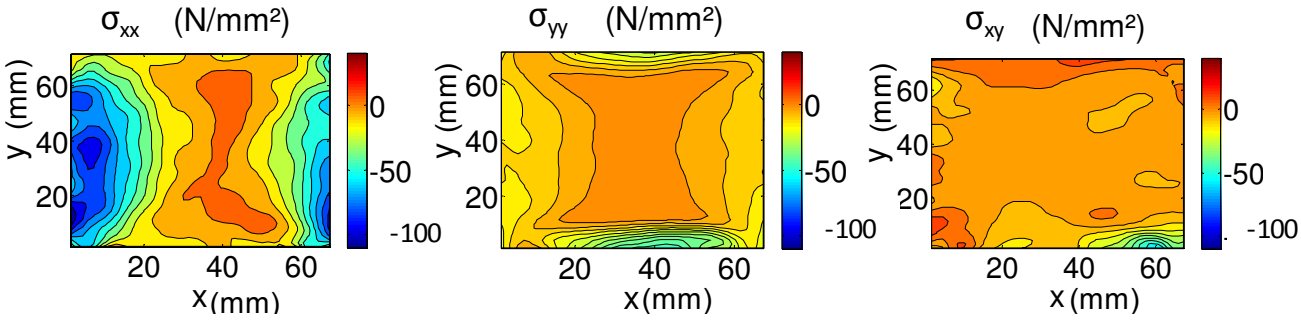

Figure 6. Maps of the components of the stress field at $\varepsilon = 3\%$.

Conclusion

A 3D Digital Image Stereocorrelation technique method was used to analyse the buckling behaviour of box panels during their compression. This technique is highly efficient to provide relevant data on the 3D displacement and strain fields at the surface of the box panels. The analysis of the 3D displacement field provides information on the buckling behaviour of the studied panel. This permitted also to highlight the influence of scores and flaps on this phenomenon. The analysis of the strain field shows that compressive strain states are mainly found to be compressive along the box edges, whereas the central zone is nearly not loaded during the compression. The analysis of the stress field reveals that the regions along the vertical edges are the most stressed zones and emphasizes that the boundary conditions have to be accurately determined in order to predict the buckling behaviour of box panels. This analysis is one part of a large work which investigates the effect of residual stresses, box erection, as well as box compression on the stress field calculated in the outer liner. The effect of box geometries was also investigated. Finally, it provides data that can be used as input for post-buckling analytical or numerical models in order to optimize the box design.

Acknowledgments

The authors would like to thank Cartonneries de Gondardennes (Wardrecques, France) for supplying corrugated boards and the long-term research program “Heterogeneous Fibrous Materials” of the European Synchrotron Radiation Facility (Grenoble, France).

References

[1] J. Viguié, P.J.J. Dumont, I. Desloges, E. Mauret: Packag. Technol. Sci. (2010), on line

[2] R. C. Mc Kee, J. W. Gander, J.R. Wachuta: Paperboard Packag. Vol. 48(8) (1963) p. 149.

[3] T.J. Urbanik: Develop. Validat. Appl. Inelastic Method. Struct. Anal. Des., Vol. 343 (1996) p. 85

[4] L. Beldie, G. Sandberg, L. Sandberg: Packag. Technol. Sci., Vol. 15 (2001), p. 1

[5] M.E. Biancolini, C. Brutti: Technol. Sci., Vol. 16 (2003), p. 47

[6] J.L. Thorpe and D. Choi: Tappi Journal, Vol 75(7) (1992), p. 155

[7] L. Meunier, G. Chagnon, D. Favier, L. Orgéas, P. Vacher: Polym. Test., Vol. 27 (2008), p.765

[8] J.-J. Orteu: Optics and Lasers in Engineering, Vol. 47 (2009), p. 282

[9] P. Vacher, S. Dumoulin, F. Morestin, S. Mguil-Touchal: Instn Mech Engrs Part C ImechE, Vol. 213 (1999), p. 811

[10] T. Couderc, Phd Thesis, Université de Savoie, Annecy, France (2005)

[11] J. Viguié, Phd Thesis, Institut polytechnique de Grenoble (Grenoble INP), Grenoble, France (2010)